Table of Contents:

Section S1. Materials, method and synthesis

Materials

All chemicals and solvents were used as received without any further purification. Completion of reactions was determined by TLC using silica gel covered aluminum plates (Merck 60, F-254) and visualized by UV detection (λ = 254 nm). Purification by column chromatography was performed using silica gel (0.063–0.2 mm, 100 mesh ASTM) from PENTA s.r.o. (Prague, CZ). Anhydrous $CHCl_3$, Et_2O and MeOH, boron trifluoride diethyl etherate, benzene-1,4-diboronic acid, $Pd(PPh_3)_4$ were purchased from Sigma-Aldrich. Anhydrous dichloroethane and toluene were purchased from Acros Organics. 4-bromoacetophenone, 4-bromobenzaldehyde and $P(SiMe_3)_3$ were purchased from ABCR (Karlsruhe, Germany). Mercury (II) acetate and acetonitrile were purchased from VWR. NaOH and K_2CO_3 were purchased from PENTA s.r.o. Hexane, CH_2Cl_2, 1,4-dioxane, ethanol, $CHCl_3$, MeOH, THF were purchased from Lach-Ner s.r.o.

Methods

Nuclear magnetic resonance (NMR) spectra of small molecules were measured on Bruker Advance 400 MHz / 500 MHz spectrometer.

High resolution mass (HR-MS) spectrometry was performed on a Agilent 5975B MSD coupled to 6890N gas chromatograph using atmospheric-pressure chemical ionization (APCI) as ionization method.

Solid-state (ss) NMR spectra of polymer were recorded by ^{31}P magic angle spinning (MAS) with MAS rate of 13 kHz using 3.2 mm diameter zirconia rotors (contact time 10 ms and relaxation delay 5.0 s), and ^{13}C cross polarization magic angle spinning (CP/MAS) with MAS rate of 20 kHz and using 4 mm diameter zirconia rotors (contact time 10 ms and relaxation delay 5.0 s).

Fourier transform infrared (FTIR) spectra of materials were obtained as materials/KBr mixture pellets on an AVATAR 370 FTIR spectrometer from Thermo Nicolet.

Elemental analyses (EA) of C, H and N were carried out via a PE 2400 Series II CHN Analyzer. The mass percentage of other elements were characterized by optical emission spectrometry (OES) with radial observation of inductively coupled plasma (ICP) using SPECTRO Arcos spectrometer.

Electron paramagnetic resonance (EPR) spectra were recorded on a Bruker EMX^{plus} 10/12 CW (continuous wave spectrometer) equipped with Premium-X-band microwave-bridge. Quartz tubes with 3 mm i.d. (Bruker) were used to measure either powder-samples or corresponding toluene suspension, which was prior to measurement sonicated in ultra-sonic bath. The sample-containing tube was finally inserted into either ER-4102003 ST-LC (standard rectangular) or ER-4119001 HS-W1 (high sensitivity) cavity (both Bruker). The experimental g-factor was determined using a built-in spectrometer frequency counter and an ER-036TM NMR-Teslameter (both Bruker).

Aggregation structure of polymer was characterized via powder X-ray diffraction (PXRD) using Bruker AXS D8 Advanced SWAX diffractometer with Cu Kα (λ = 0.15406 nm) as a radiation source.

Porosity of materials was tested by nitrogen adsorption/desorption using a Autosorb iQ instrument with Helium mode. Samples for nitrogen sorption at 77 K were degassed at 120 °C for 24 h under vacuum (10^{-5} Bar) before analysis. Brunauer-Emmett-Teller (BET) surface area (S_{BET}) was calculated in relative pressure range (p/p_0) from 0.05 to 0.35. Pore size distribution was calculated using NLDFT Model.

The small and wide angle X-ray scattering (SAXS/WAXS) measurements were performed using a Xenocs Nano-inXider-SW, with a microfocus X-ray tube with a copper target.

The morphology of samples was characterized using scanning electron microscopy (SEM) on Nova NanoSEM 450 microscope from FEI. Energy-dispersive X-ray spectroscopy (EDX) was examined using EDAX Metek Octane Pro Detector.

Transmission Electron Microscope (TEM) images and selected area electron diffraction (SAED) were performed on a JEM-1011 instrument (JEOL) by operating at 80 kV accelerating voltage with a spherical aberration coefficient of 5.6 mm. Images were recorded on VELETA-side-mounted TEM CCD (charge-coupled device) camera with a resolution of 2K x 2K.

Optical properties of polymer were obtained by solid state UV/Vis measurements on Cary 6000i UV-Vis-NIR spectrometer from Agilent, and solid state fluorescence measurements recorded on Fluorolog FL3-22 fluorometer (Horiba-Jobin Yvon). Luminescence quantum yields were determined absolutely using the commercial integrating sphere setup Quantaurus-QY C11347-11 from Hamamatsu.

Thermogravimetry analysis (TGA) was carried out on Setsys Evolution 18 thermal analyzer from Setaram under air and nitrogen atmosphere with the heating rate of 10 ^{o}C/min.

Synthesis of 1,3-Bis(4-bromophenyl)prop-2-en-1-one (1)

Preparation procedure was a modified method based on two relevant literatures.[1, 2] 4-bromoacetophenone (17.2 g, 86.4 mmol) and 4-bromobenzaldehyde (16 g, 86.4 mmol) were dissolved in 120 mL ethanol with constant stirring. Solution of NaOH (1.2 g, 30.0 mmol) in 22 mL H_2O was added, and the reaction was kept stirring at room temperature overnight. The mixture was filtered and washed with water and 60 mL ethanol. The white filter cakes were recrystallized from ethanol/$CHCl_3$ (1/1) overnight to form green/yellow product 1,3-Bis(4-bromophenyl)prop-2-en-1-one (**1**) 28.2 g (77.0 mmol for $C_{15}H_{10}Br_2O$, 89.1 % yield). ^{1}H NMR (400 MHz, $CDCl_3$): 7.93-7.87 (2H, m), 7.77 (1H, d, J= 15.7 Hz), 7.70-7.65 (2H, m), 7.61-7.56 (2H, m), 7.55-7.51 (2H, m), 7.49 (1H, d, J= 15.7 Hz).

Synthesis of 2,4,6-tri(4-bromophenyl)pyrylium tetrafluoroborate (2)

Preparation procedure was a modified method based on three related literatures.[3-5] Compound **1** (24.29 g, 66.4 mmol) and 4-bromoacetophenone (11.23 g, 56.4 mmol) were purged under argon and mostly dissolved in 160 mL anhydrous dichloroethane. Boron trifluoride diethyl etherate (19.7 mL, 159.4 mmol) was added. The mixture was stirred and refluxed under argon atmosphere for 18 h. After the mixture was cooled to room temperature, 300 mL anhydrous Et_2O was added to form more precipitates. Subsequently, the precipitate was filtered and washed with anhydrous Et_2O and anhydrous $CHCl_3$ separately. The yellow powders were dried under vacuum to afford 2,4,6-tri(4-bromophenyl)pyrylium tetrafluoroborate (**2**) 9.57 g (15.1 mmol for $C_{23}H_{14}BBr_3F_4O$, 26.7% yield). ^{1}H NMR (500 MHz, $(CD_3)_2CO$): 9.32 (2H, s), 8.64-8.59 (4H, m), 8.55-8.52 (2H, m), 8.06-8.04 (2H, m), 8.04-8.00 (4H, m). ^{13}C NMR (125.7 MHz, $(CD_3)_2CO$): 170.61, 165.54, 133.30, 132.05, 131.57, 130.57, 130.48, 130.30, 128.44, 116.02.

Section S2. NMR data for synthesizing monomers

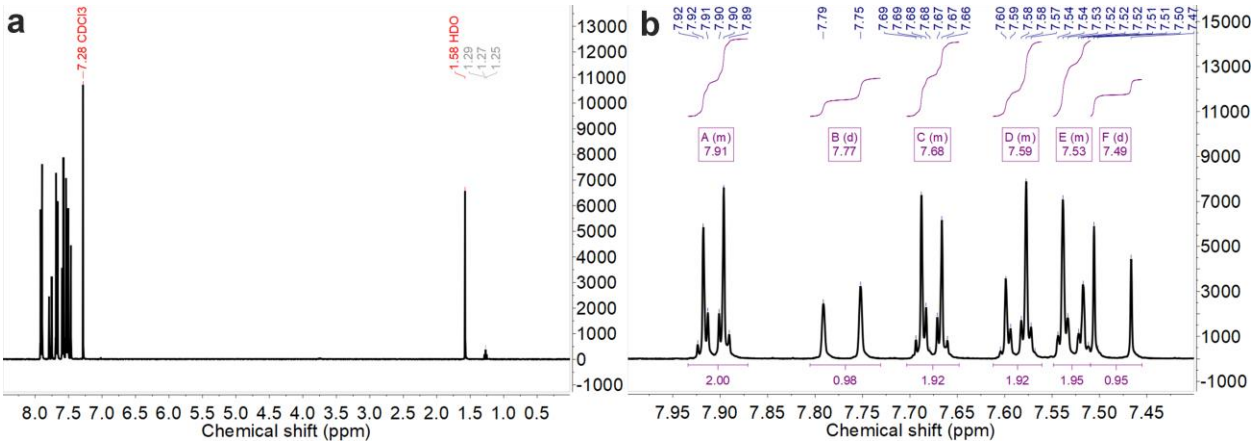

Figure S1. ^{1}H-NMR spectrum of 1,3-Bis(4-bromophenyl)prop-2-en-1-one (**1**) in $CDCl_3$: (a) original full spectrum; (2) spectrum with analysis.

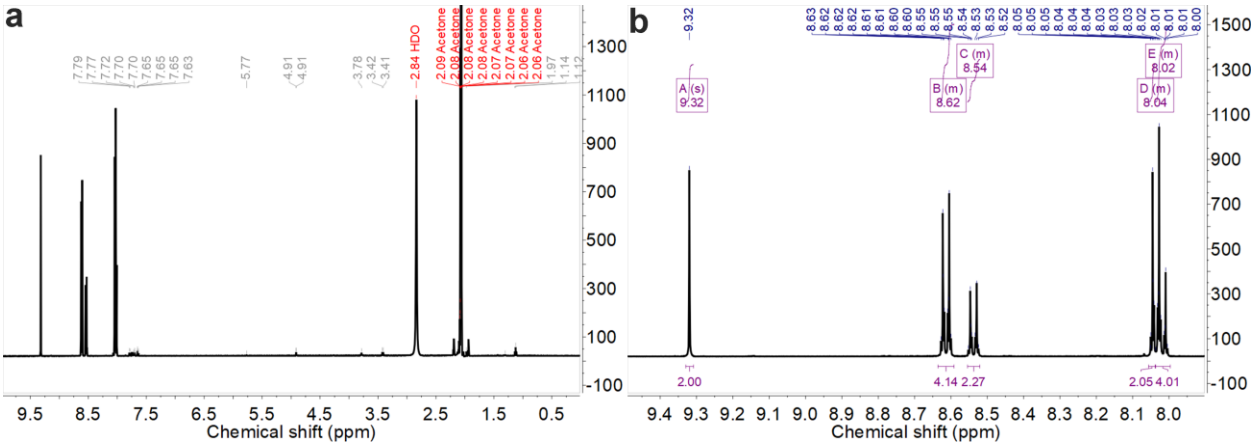

Figure S2. ^{1}H-NMR spectrum of 2,4,6-tri(4-bromophenyl)pyrylium tetrafluoroborate (**2**) in $(CD_3)_2CO$: (a) original full spectrum; (2) spectrum with analysis.

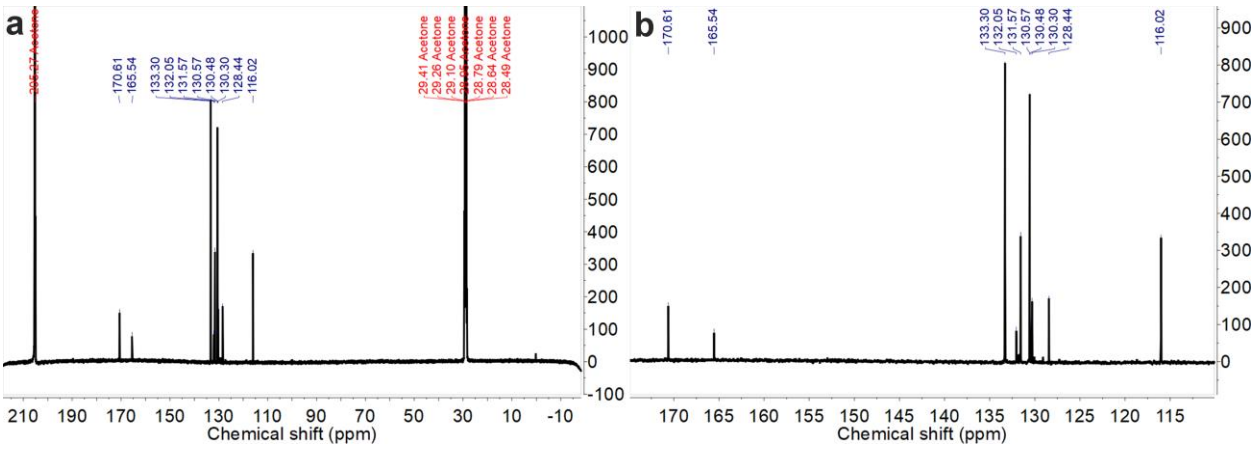

Figure S3. ^{13}C-NMR spectrum of 2,4,6-tri(4-bromophenyl)pyrylium tetrafluoroborate (**2**) in $(CD_3)_2CO$: (a) original full spectrum; (2) zoom-in spectrum.

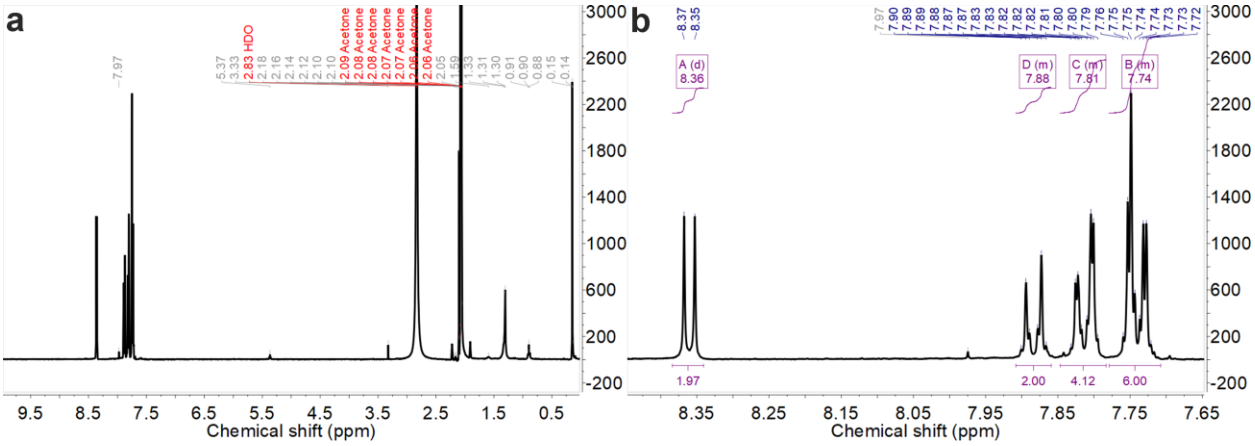

Figure S4. ^{1}H-NMR spectrum of 2,4,6-tri(4-bromophenyl)-λ^3-phosphinine (**3**) in $(CD_3)_2CO$: (a) original full spectrum; (2) spectrum with analysis.

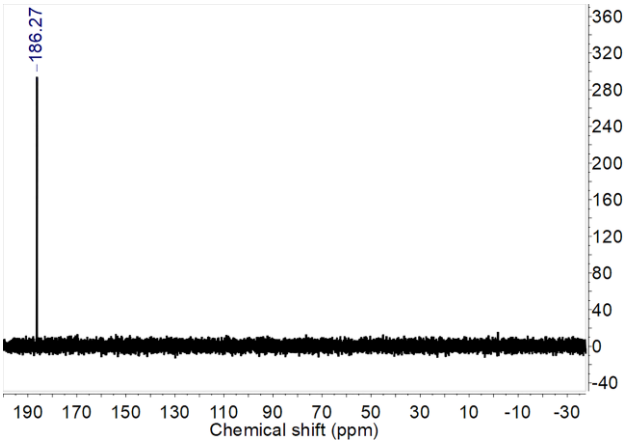

Figure S5. ^{31}P-NMR spectrum of 2,4,6-tri(4-bromophenyl)-λ^3-phosphinine (**3**) in $(CD_3)_2CO$.

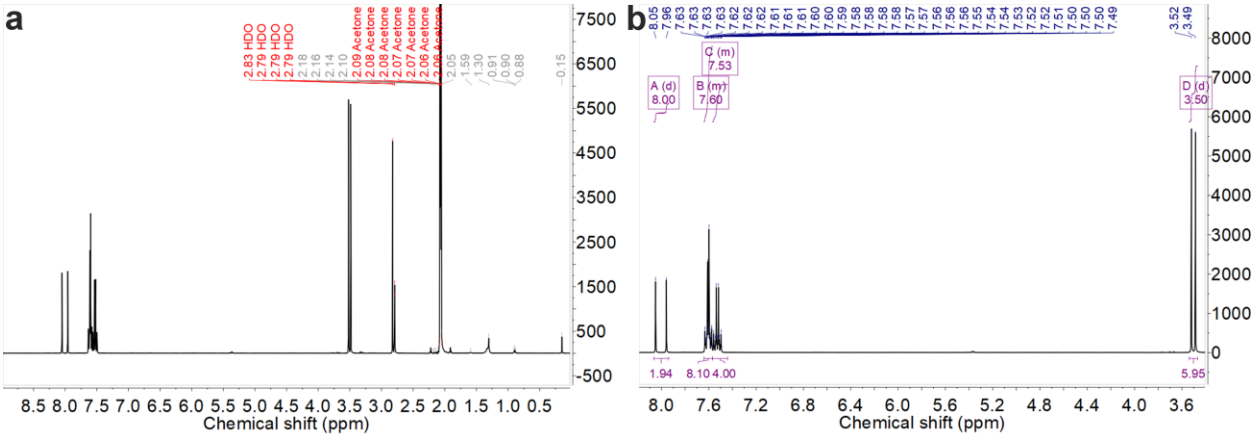

Figure S6. ^{1}H-NMR spectrum of 1,1-dimethoxy-2,4,6-tri(4-bromophenyl)-λ^5-phosphinine (**4**) in $(CD_3)_2CO$: (a) original full spectrum; (2) spectrum with analysis.

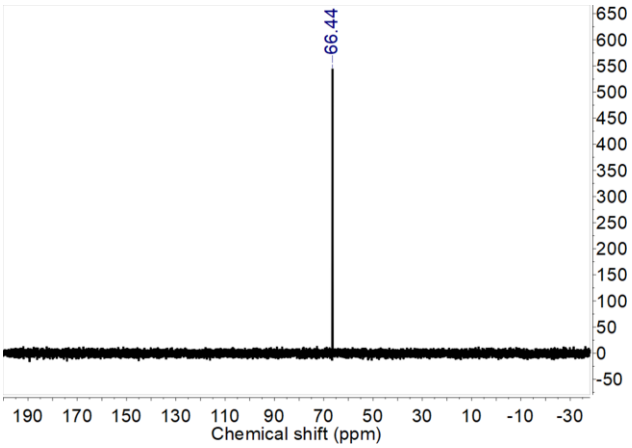

Figure S7. ^{31}P-NMR spectrum of 1,1-dimethoxy-2,4,6-tri(4-bromophenyl)-λ^5-phosphinine (**4**) in $(CD_3)_2CO$.

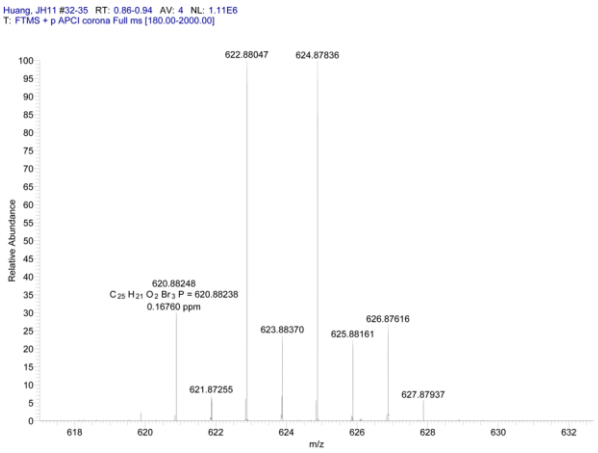

Figure S8. Mass (APCI) spectrum of 1,1-dimethoxy-2,4,6-tri(4-bromophenyl)-λ^5-phosphinine (**4**).

Section S3. Procedure for checking stability of 3 or 4 with solvent or catalyst.

Table S1. Common synthetic protocols for the preparation of covalent phosphinine-based polymers.

Coupling reaction	Solvent	Catalyst	Temperature	Reactive groups
Sonogashira-Hagihara coupling [6]	DMF	$Pd(PPh_3)_4$ /CuI/ Triethylamine	100 ºC	Bromophenyl / Ethynylphenyl
Ullmann coupling [7]	DMF or Pyridine	Cu or CuI	Reflux	Bromophenyl / Bromophenyl
Suzuki-Miyaura coupling [8]	Toluene or 1,4-Dioxane	$Pd(PPh_3)_4$/ K_2CO_3	Reflux	Bromophenyl / Boronic acid
Stille coupling [9]	Toluene or Mesitylene	$Pd(PPh_3)_4$	Reflux	Bromophenyl / Trimethylstannyl
Glaser coupling [10]	Pyridine	Cu or CuI	60 ºC	Ethynylphenyl / Ethynylphenyl
Trimerization of nitrile [11]	CH_2Cl_2	Triflic acid	R. T.	Nitrile /Nitrile /Nitrile

3 or **4** were mixed with corresponding solvents and catalysts via continuous stirring, and the mass ratio of chemicals and solvents were calculated according to relevant references [6-11]. Then the solution was heated to a certain temperature overnight. After cooling down, the solvent was removed by using rotary evaporator. The residue was collected for ^{31}P NMR in $(CD_3)_2CO$. It is worth noting that the P might be removed if it formed some compounds with low boiling point.

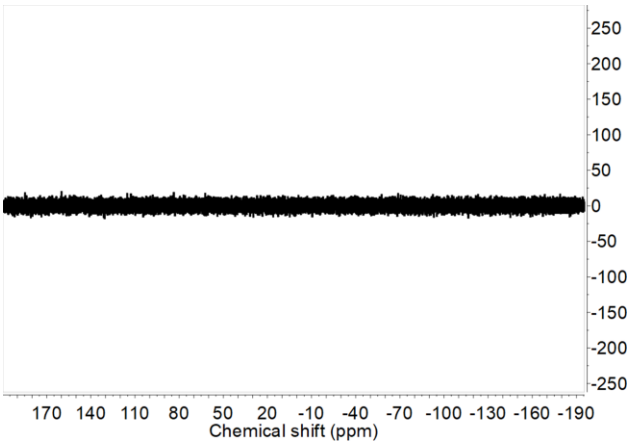

Figure S9. ^{31}P NMR spectrum of **3** after mixing with DMF at 100 ^{o}C.

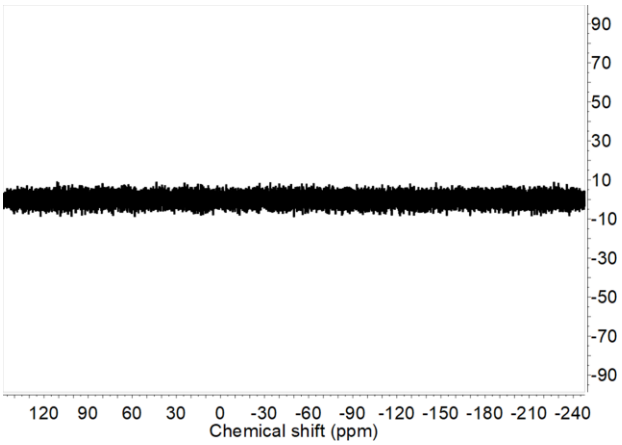

Figure S10. ^{31}P NMR spectrum of **4** after mixing with DMF at 100 ^{o}C.

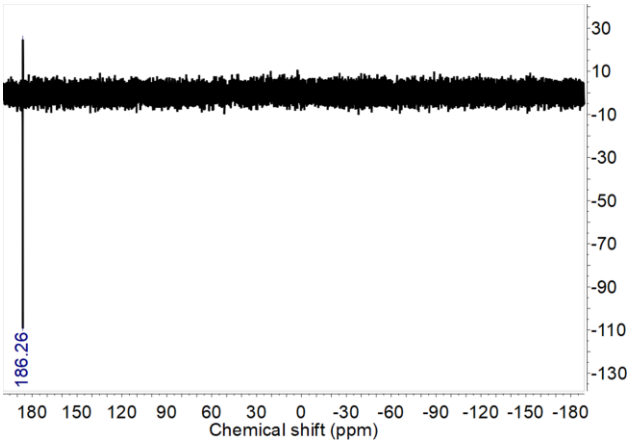

Figure S11. ^{31}P NMR spectrum of **3** after mixing with pyridine at 60 ^{o}C.

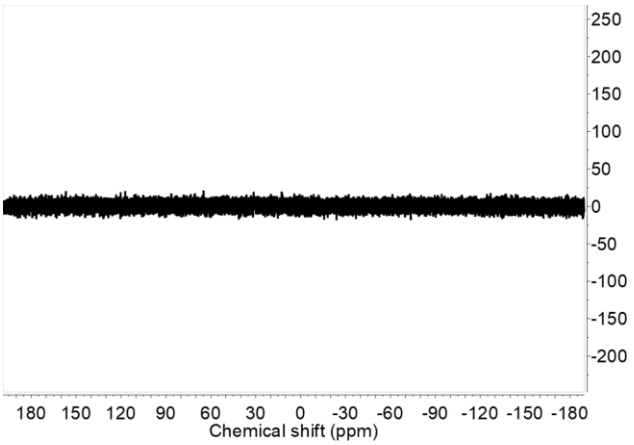

Figure S12. ^{31}P NMR spectrum of **4** after mixing with pyridine at 60 ^{o}C.

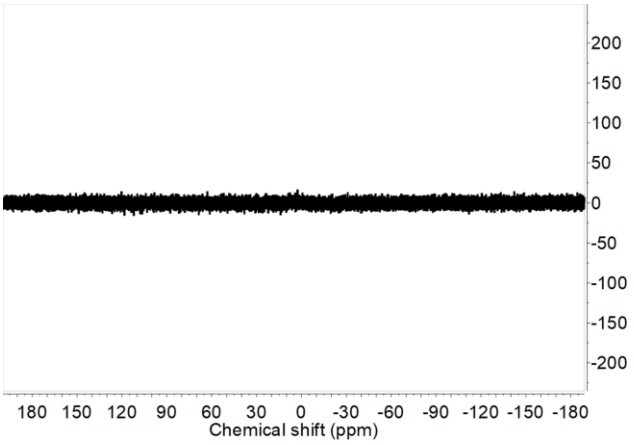

Figure S13. ^{31}P NMR spectrum of **3** after mixing toluene and triethylamine for refluxing.

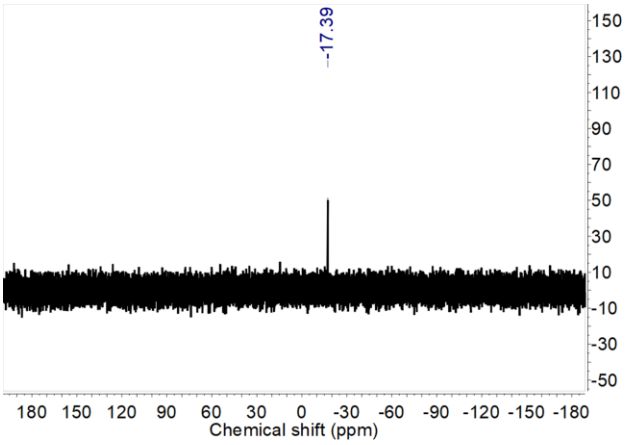

Figure S14. ^{31}P NMR spectrum of **4** after mixing toluene and triethylamine for refluxing.

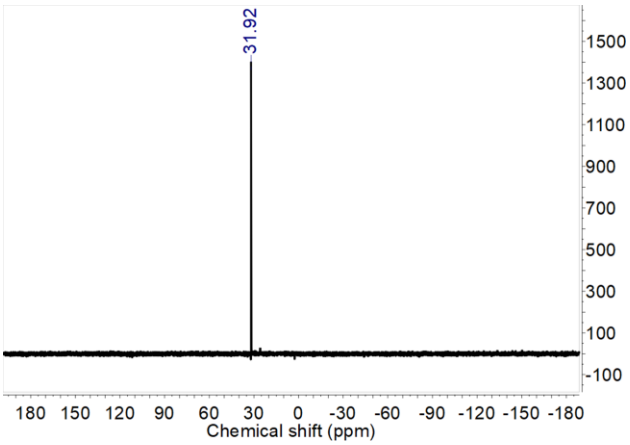

Figure S15. ^{31}P NMR spectrum of **3** after mixing with toluene and $Pd(PPh_3)_4$ for refluxing.

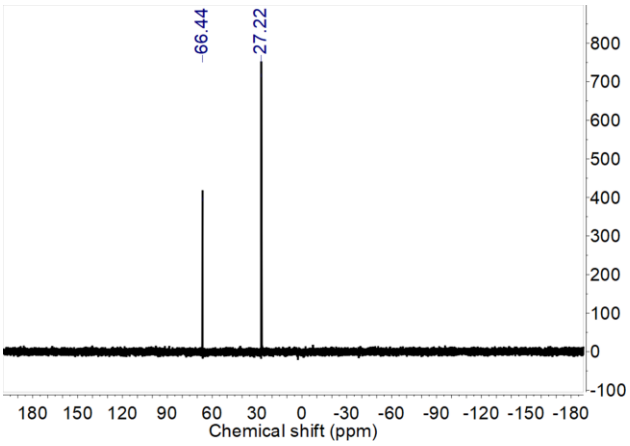

Figure S16. ^{31}P NMR spectrum of **4** after mixing with toluene and $Pd(PPh_3)_4$ for refluxing.

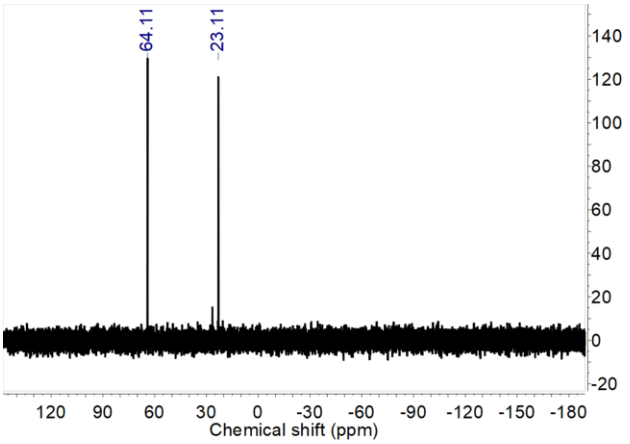

Figure S17. ^{31}P NMR spectrum of **4** after mixing with toluene and $Pd(PPh_3)_4$ /K_2CO_3 for refluxing.

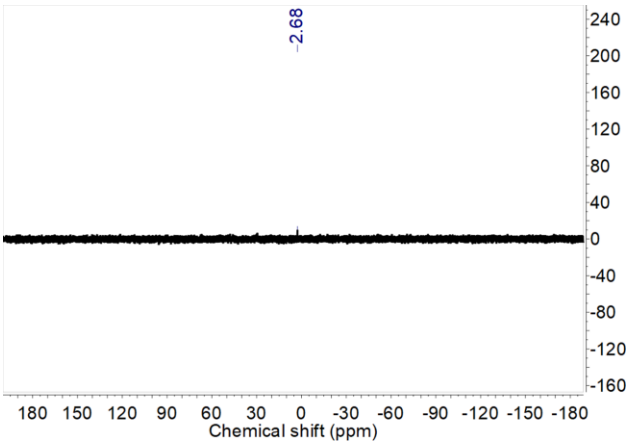

Figure S18. ^{31}P NMR spectrum of **3** after mixing with CH_2Cl_2 and triflic acid at R.T.

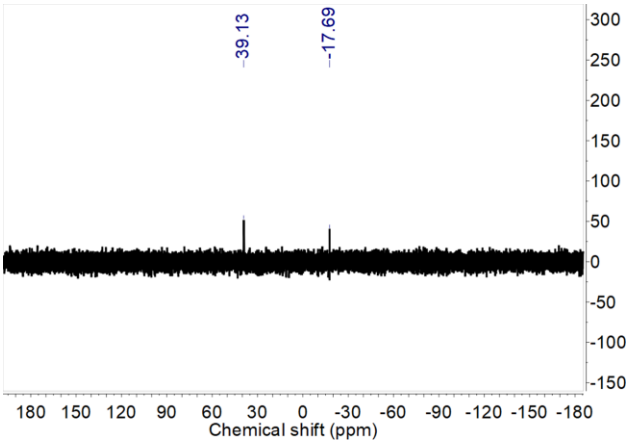

Figure S19. ^{31}P NMR spectrum of **4** after mixing with CH_2Cl_2 and triflic acid at R.T.

Table S2. Stabilities of 2,4,6-tri(4-bromophenyl)-λ^3-phosphinine (3) and 1,1-dimethoxy-2,4,6-tri(4-bromophenyl)-λ^5-phosphinine (4) according to ^{31}P NMR in section S3.

Solvent	Catalyst	Temperature	Stability of **3**	Stability of **4**
DMF	-	100 °C	No	No
Pyridine	-	60 °C	No	No
Toluene	Et_3N	Reflux	No	No
Toluene	$Pd(PPh_3)_4$	Reflux	No	Yes
Toluene	$Pd(PPh_3)_4$ /K_2CO_3	Reflux	[a]	Yes
CH2Cl2	Triflic acid	R. T.	No	No

[a] This experiment was not carried out, since 3 was shown to be unstable in the presence of $Pd(PPh_3)_4$.

Section S4. Procedure for synthesizing phosphinine model compound (PMC).

Procedure (Figure S20) is similar to the Suzuki-Miyaura coupling polymerization.[8, 12, 13] Monomer **4** (50 mg, 0.0802 mmol), phenylboronic acid (29.4 mg, 0.241 mmol) and catalyst $Pd(PPh_3)_4$ (6.95 mg, 0.00601 mmol) were added to a 100 mL three-neck flask and purged under argon. 11 mL 1,4-dioxane was degassed by argon bubbling for 20 min and then was added to flask with continuous stirring. 1.7 mL aqueous K_2CO_3 solution was degassed by argon bubbling for 20 min and then was added to flask. After being degassed by argon bubbling for further 30 min, the mixture was stirred and refluxed under argon atmosphere overnight. Crude PMC, labelled as PMC-C, was obtained.

Half amount of PMC-C (43.2 mg) was purified by column chromatography on silica gel (eluent hexane/CH_2Cl_2 = 65/35), and then was recrystallized in hot acetonitrile to afford pure model compound 11.4 mg (0.0185 mmol for $C_{43}H_{35}O_2P$, 46.2% yield), labelled as PMC. MS (APCI):

calcd for [$C_{43}H_{35}O_2P$] 615.24474, found 615.24437. ^{1}H NMR (400 MHz, benzene-d_6): 8.28 (2H, d, J= 36.8 Hz), 7.82-7.73 (4H, m), 7.72-7.54 (14H, m), 3.14 (6H, d, J= 13.9 Hz), Note: peaks at 7.36-6.94 ppm are mixed with peaks of benzene and accordingly cannot be quantified. ^{31}P NMR (162 MHz, benzene-d_6): 68.22. ^{13}C NMR (151 MHz, benzene-d_6): 142.40, 142.39, 141.26, 140.90, 139.01, 138.94, 138.72, 137.81, 137.67, 137.63, 128.83, 128.76, 127.23, 127.17, 127.10, 126.92, 126.85, 126.10, 115.82, 94.14, 93.24, 51.84, Note: signals at 128.83-126.10 ppm are mixed with peaks of benzene-d_6. The spectra were shown in Figure S21, S22, 4e, and 4f.

According to mass, ^{1}H NMR and ^{31}P NMR spectra, the structure of model compound after purification (PMC) was confirmed. ^{13}C NMR spectrum of PMC shows the characteristic peaks of phosphinine structure: 115.82 (para-C of P), 94.14 /93.24 (ortho-C of P), 51.84 (C of MeO.[14]

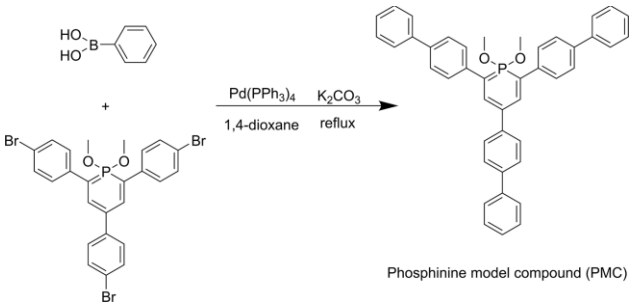

Figure S20. Suzuki-Miyaura coupling route for synthesizing phosphinine model compound (PMC).

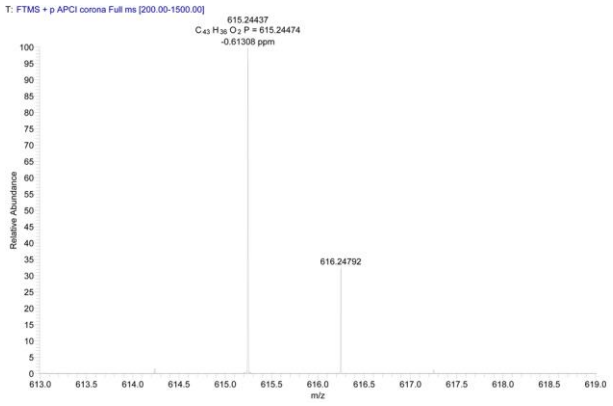

Figure S21. Mass (APCI) spectrum of PMC.

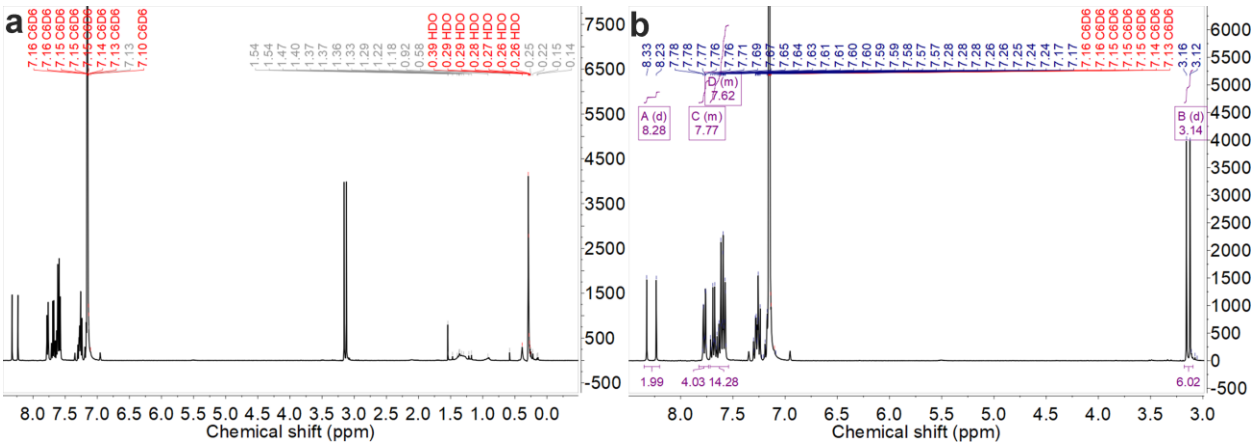

Figure S22. ^{1}H-NMR spectrum of PMC in benzene-d_6: (a) original full spectrum; (2) spectrum with analysis.

In ^{31}P NMR spectrum of crude PMC (PMC-C), the signal at δ = 68.22 ppm is characteristic for λ^5-phosphinine,[15] and it can be further confirmed by comparison with the only one signal in ^{31}P NMR spectrum of PMC (Figure 2c). Another signal at δ = 28.29 ppm in ^{31}P NMR spectrum of PMC-C is corresponding to the signal of remaining Ph_3PO (Figure S24), which is always formed during the decomposition of $Pd(PPh_3)_4$ catalyst.

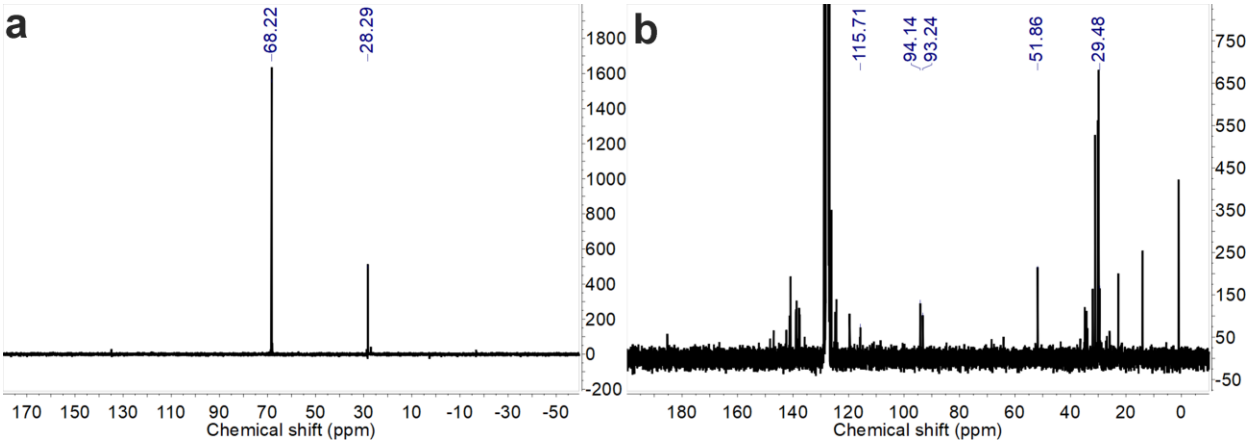

Figure S23. (a) ^{31}P NMR spectrum of PMC-C in benzene-d_6; (b) ^{13}C NMR spectrum of PMC-C in benzene-d_6;

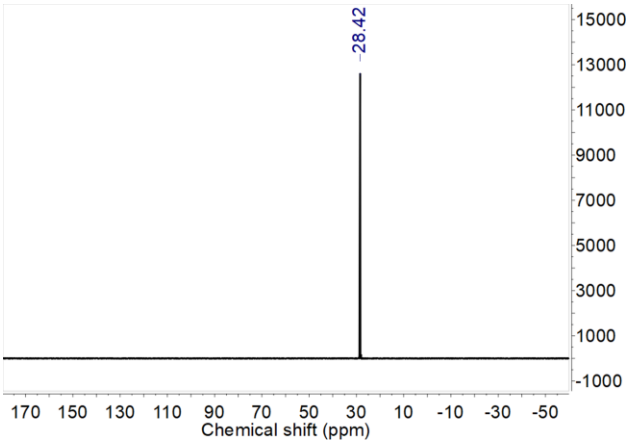

Figure S24. ^{31}P-NMR spectrum of Ph_3PO in benzene-d_6.

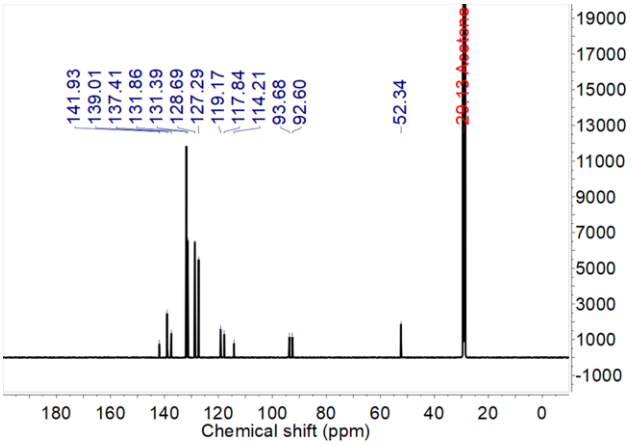

Figure S25. ^{13}C-NMR spectrum of 1,1-dimethoxy-2,4,6-tri(4-bromophenyl)-λ^5-phosphinine (**4**) in $(CD_3)_2CO$.

Monomer **4**, ^{13}C-NMR (126 MHz, $(CD_3)_2CO$): 141.93, 139.01, 137.41, 131.86, 131.39, 128.69, 127.29, 119.17, 117.84, 114.21, 93.68, 92.60, 52.34.

Section S5. Structure, composition and morphology data of CPF-1

Table S3. Composition of CPF-1 by combustion elemental analysis (EA) and inductively coupled plasma - optical emission spectrometry (ICP-OES) (in wt%).

	C	N	H	O	P	Pd	Br	B	K
Calculated	82.07	0	5.28	6.43	6.22	0	0	0	0
CPF-1	73.47	0	4.82	-	5.67	0.19	1.32	0.01	0.3

CPF-1-48h is a controlled polymer sample prepared by the same synthetic route and cleaning procedure. The difference is this reaction ran only for 48 h, while CPF-1 was obtained after 80 h. With a shorter polymerization time, CPF-1-48h contains 5.66 wt% unreacted Br end group, while CPF-1 contains 1.32 wt% Br. Besides, the surface area of CPF-1-48h is 18.89 m^2 g^{-1}, while CPF-1 shows much larger surface area of 72.4 m^2 g^{-1}. All the evidences revealed CPF-1 is a more completely polymerized framework structure than CPF-1-48h. In ^{31}P MAS ssNMR spectrum of CPF-1-48h, the intensity of phosphorus peak assigned to Ph_3PO are much lower than that in CPF-1, which revealed that a more complete framework structure will trap more Ph_3PO in polymer

Table S4. Composition of CPF-1-48h by combustion elemental analysis (EA) and inductively coupled plasma - optical emission spectrometry (ICP-OES) (in wt%).

	C	N	H	O	P	Pd	Br	B	K
Calculated	82.07	0	5.28	6.43	6.22	0	0	0	0
CPF-1-48h	70.07	0	5.09	-	4.53	0.17	5.66	0.02	0.43

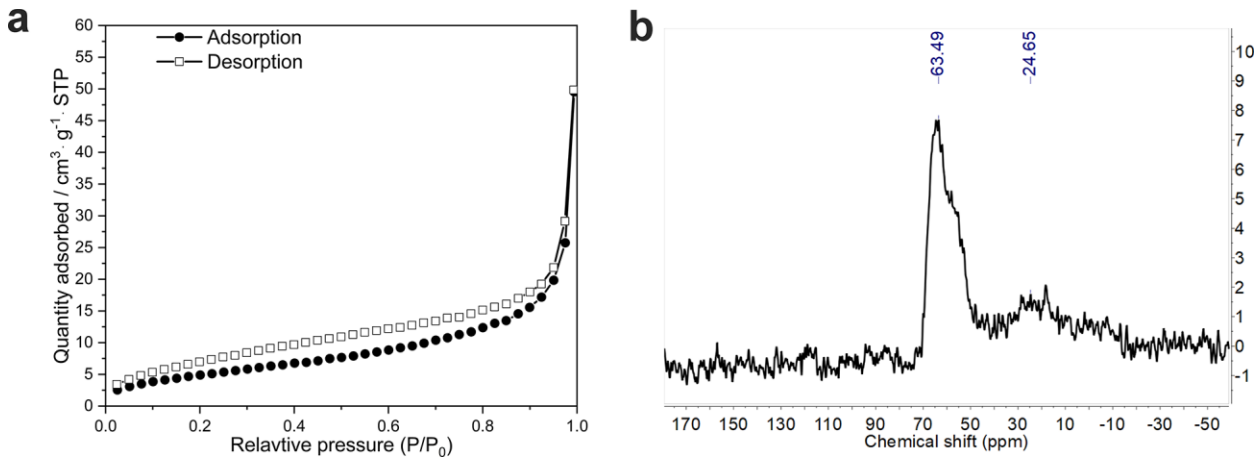

Figure S26. (a) Nitrogen sorption isotherms at 77 K and (b) ^{31}P magic angle spinning (MAS) solid-state NMR (ssNMR) spectrum of CPF-1-48h.

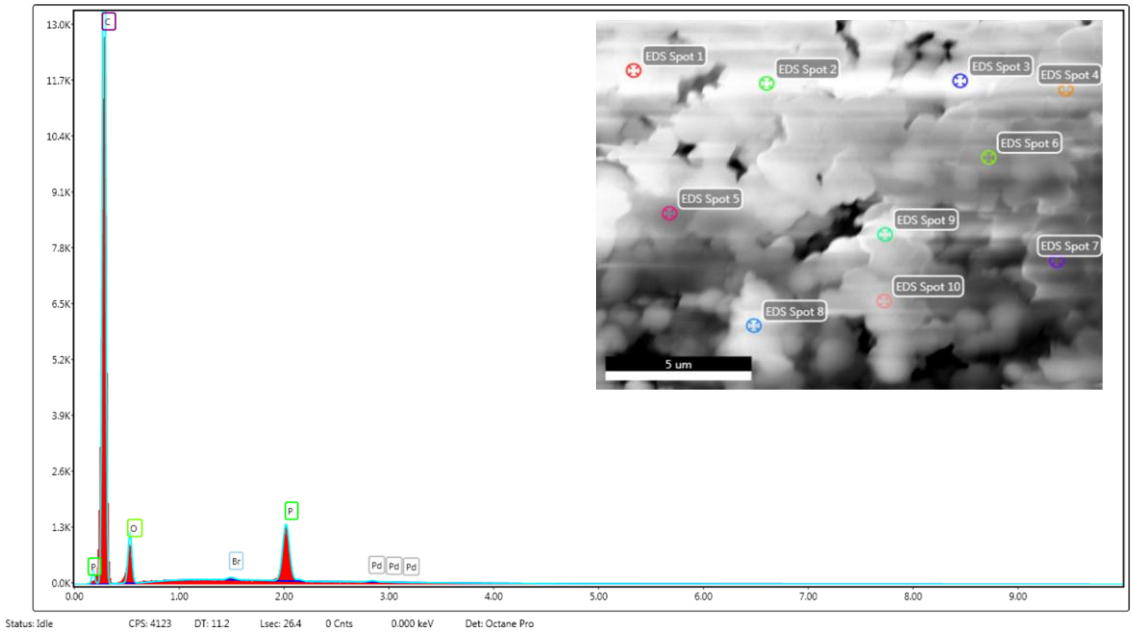

Figure S27. SEM image with EDX detected spots and EDX spectrum (spot 3) of CPF-1.

Table S5. wt% ratio of elements detected by EDX (from detected spots in Figure S26).

Items	C	N	H	O	P	Pd	Br
Calculated	82.07	0	5.28	6.43	6.22	0	0
CPF-1 Spot 1	82.43	0	-	10.55	5.61	0.76	0.65
CPF-1 Spot 2	82.60	0	-	10.66	5.34	0.78	0.62
CPF-1 Spot 3	83.09	0	-	12.14	4.30	0.28	0.19
CPF-1 Spot 4	82.88	0	-	10.96	4.96	0.61	0.58
CPF-1 Spot 5	83.16	0	-	9.89	5.45	0.76	0.75
CPF-1 Spot 6	81.63	0	-	12.20	4.88	0.70	0.59
CPF-1 Spot 7	81.41	0	-	13.84	3.68	0.54	0.52
CPF-1 Spot 8	83.54	0	-	9.31	5.77	0.78	0.60
CPF-1 Spot 9	83.01	0	-	11.60	4.38	0.52	0.48
CPF-1 Spot 10	83.83	0	-	9.89	5.09	0.69	0.50
CPF-1 Average	82.70	0	-	10.68	5.06	0.58	0.50

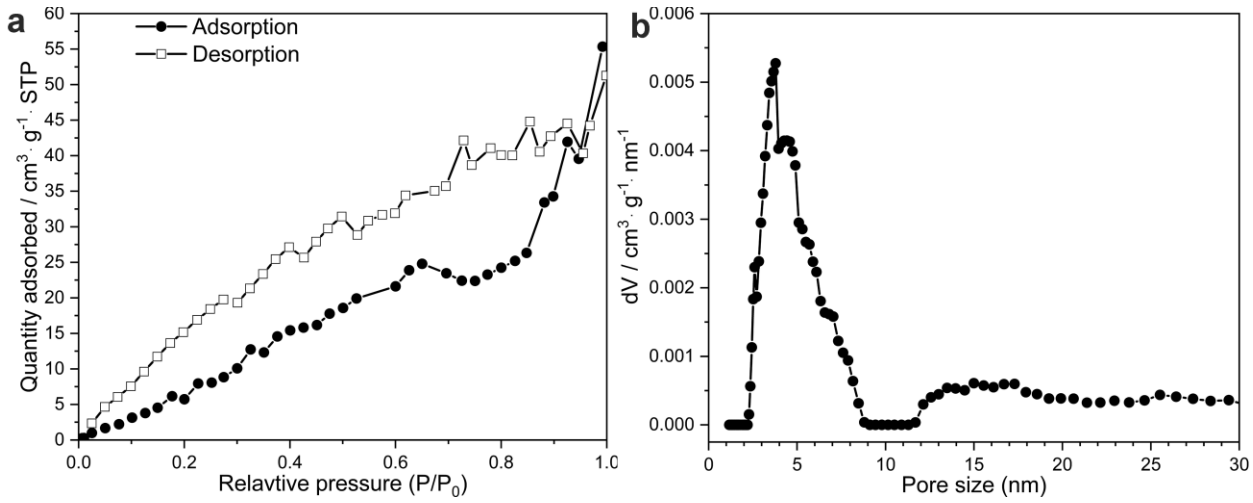

Figure S28. (a) Nitrogen sorption isotherms at 77 K and (b) NLDFT pore size distribution of CPF-1.

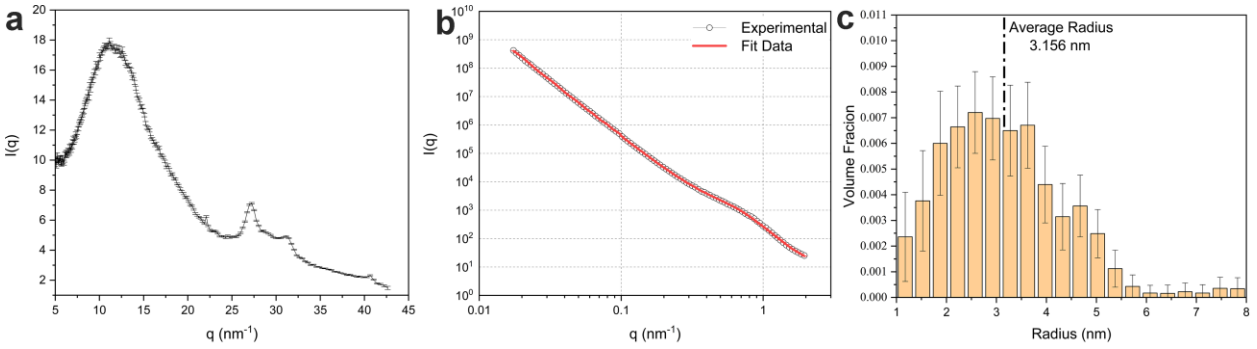

Figure S29. SAXS/WAXS data of CPF-1: (a) WAXS experimental pattern with error bar (the 3 peaks ranging from 25 to 42 nm^{-1} are derived from Pd catalyst lattice); (b) SAXS experimental pattern/fit data; (c) radius distribution collected from SAXS patterns using a minimum assumption Monte Carlo method.[16, 17]

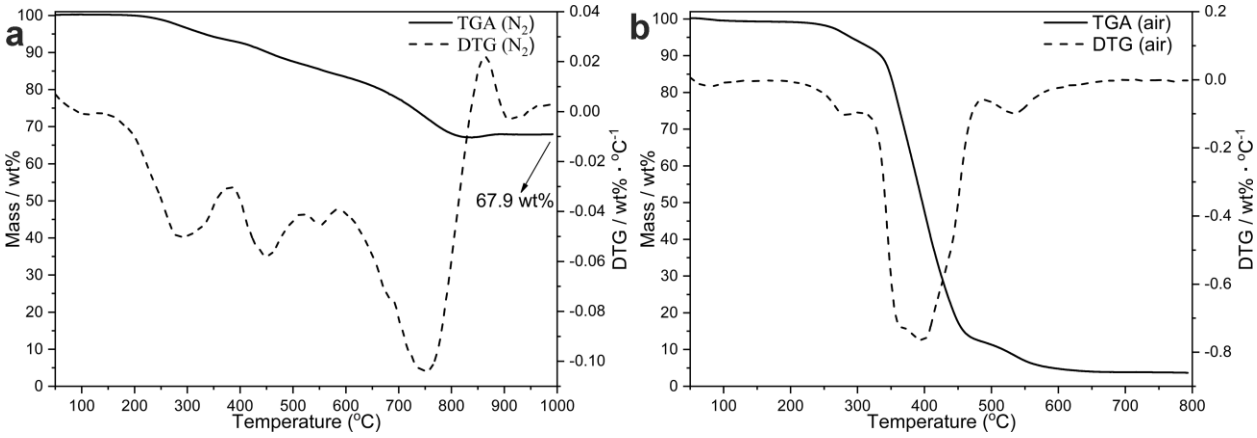

Figure S30. (a) Thermogravimetric analysis measurements of CPF-1 (a) under N_2 and (b) under air atmosphere.

Section S6. Discussion and data for electronic properties of CPF-1

Conductivity measurements: Electrical conductivity was determined by two-point I-V measurements. Powder samples were pelletized into a disk between two stainless rods supported by an insulating plastic insert with an inner diameter of 8 mm. I-V profiles were obtained and

recorded at RT using a source meter, Keithley 2612 A, with the voltage ranging -10 to 10 V in typical experiments. Average of minimum three separate measured current values was analyzed to calculate the conductivity of each sample.

EPR discussion for monomer 4 and CPF-1.

Methods of Computation

The DFT computations were performed within the Gaussian 09 quantum chemical package (version D.01).[18] The geometry of monomer **4** radical cation was optimized at the B3LYP/6-31+G(d,p) level. The EPR parameters such as g-factor and hyperfine coupling constants, A, were calculated by the PBE0/EPR-III(C,H,O)/IGLO-III(P)/Def2-TZVP(Br) [19-23] using the conducting polarizable continuum model (C-PCM) [24] for toluene.

Simulations of the ERP spectra were acquired with the MATLAB toolbox EasySpin v. 5.2.13. by least-square fitting to an experimental spectrum using a combination of Nelder-Mead simplex and particle swarm algorithms.[25] Instrumental parameters such as microwave frequency, central field, sweep-width, number of points and modulation amplitude were included in the simulation

Discussion

Figure S31 shows the EPR spectra of monomer **4** radical cation in powdered form (a) and in toluene suspension (b). Both spectra display an intensive doublet and no additional signals in the range of g = 1.6 to 12.0 were found.

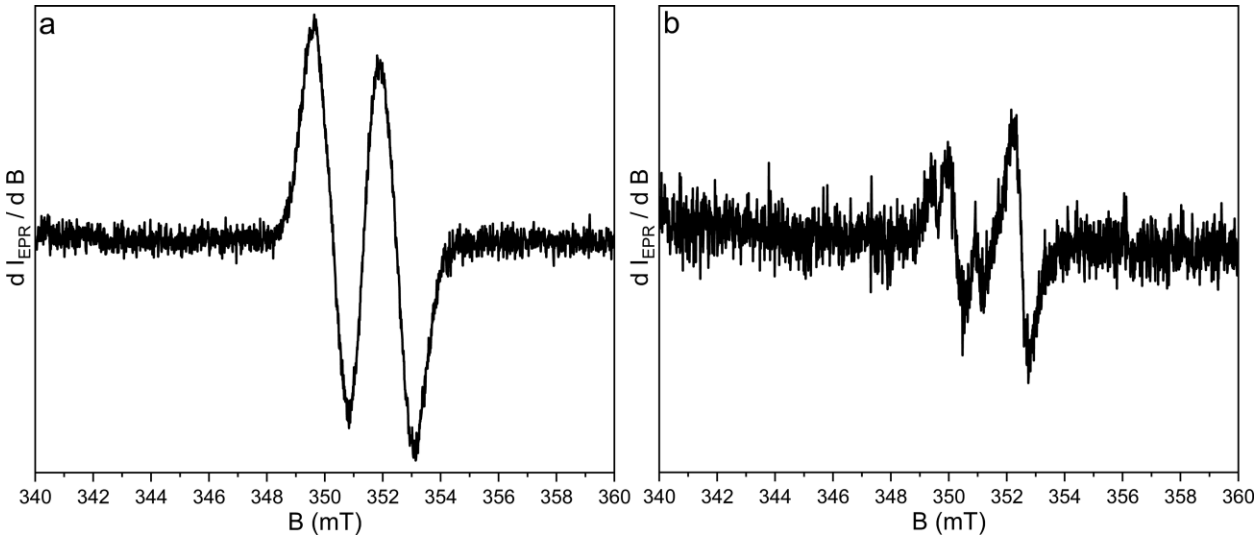

Figure S31. EPR spectra of monomer **4** (a) powder-sample b) suspension in toluene after sonication. The spectra are centered at g_{center} = 2.0040 and g_{iso} = 2.0028, respectively.

Taking into account the DFT calculations as well as simulation of the EPR spectra the doublet corresponds to hyperfine coupling/splitting coming from ^{31}P nucleus (with the average values A = 66 MHz, a = 2.36 mT). It confirms that the highest spin density is localized on central phosphinine moiety as also shown in Figure S32. This is confirmed by the DFT computed NBO spin population analysis, as well. The total spin population on phosphinine-part reads 0.65041 (including population on phosphorus atom reaching the value of 0.04412, see also Table S8).

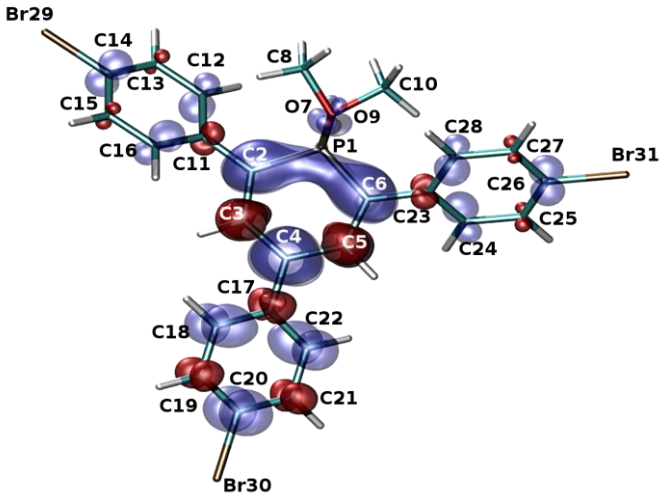

Figure S32. Visualization of total spin density for monomer **4** radical cation. Blue (red) surfaces: positive α (negative β) spin density (isovalue, 0.0024 e $Å^{-3}$).

EPR spectrum of polycrystalline monomer **4** and polymer CPF-1 are shown in Figure 4a together with simulations of their corresponding radical cation. Both spectra display rhombic symmetry (simulation parameters are summarized in Table S6).

Table S6. EPR parameters obtained from the simulation of spectra for corresponding radical cation of monomer 4 and polymer CPF-1.

Material/EPR parameter	g_1	g_2	g_3	A_1 / MHz	A_2 / MHz	A_3 / MHz
Monomeric radical cation	2.0021	2.0022	2.0085	40.218	79.926	61.394
Polymer radical cationic centers	1.9981	2.0025	2.0071	41.468	59.194	42.692

For the EPR simulation we did not consider the additional hyperfine coupling/splitting from protons, because DFT calculation shows that there are nine groups of equivalent ^1H nuclei, which have rather different A-values (Table S7). Therefore, also taking into account the anisotropy, this

will significantly increase the degrees of freedom and would bring higher uncertainties into the EPR simulations. However, the EPR spectra of polycrystalline samples can be successfully simulated considering just the hyperfine coupling/splitting from phosphorus ^{31}P (Table S6), because this shows the highest A-value by DFT calculations (Table S7). Additionally, no signals, which would point to interaction of adjacent paramagnetic centers (radical cations), forming a triplet electronic configuration, were not observed. Therefore, the majority of our paramagnetic centers are in doublet state (λ^5-phosphinine radical cations) isolated from each other, like it was already reported elsewhere.[26, 27]

Table S7. Absolute values of DFT isotropic hyperfine coupling constants of the monomer **4** radical cation (numbering of atoms/nuclei see Figure S32).

Nuclei	|A|/ MHz
1 x ^{31}P1	60.866
2 x ^{1}H(HC3,HC5)	8.150
2 x ^{1}H(HC13,HC27)	1.850
2 x ^{1}H(HC12,HC28)	3.250
2 x ^{1}H(HC16,HC24)	3.430
2 x ^{1}H(HC15,HC25)	2.016
2 x ^{1}H(HC18,HC22)	8.061
2 x ^{1}H(HC19,HC21)	4.169
3 x ^{1}H(H_3C8)	0.873
3 x ^{1}H(H_3C10)	0.873

Table S8. Natural bonding type orbital (NBO) spin populations of relevant atomic groups in radical cation of **4** calculated by DFT (numbering of atoms, see Figure S32).

Atom group	Spin population
P1	0.04412
C_5(2,3,4,5,6)H_2	0.61315
C_6(11,12,13,14,15,16)H_4Br(29)	0.05949
C_6(23,24,25,26,27,28)H_4Br(31)	0.05958
C_6(17,18,19,20,21,22)H_4Br(30)	0.17904
O(9)C(10)H_3	0.02230
O(7)C(8)H_3	0.02232

Section S7. Discussion and data for optical properties and catalytic applications of CPF-1

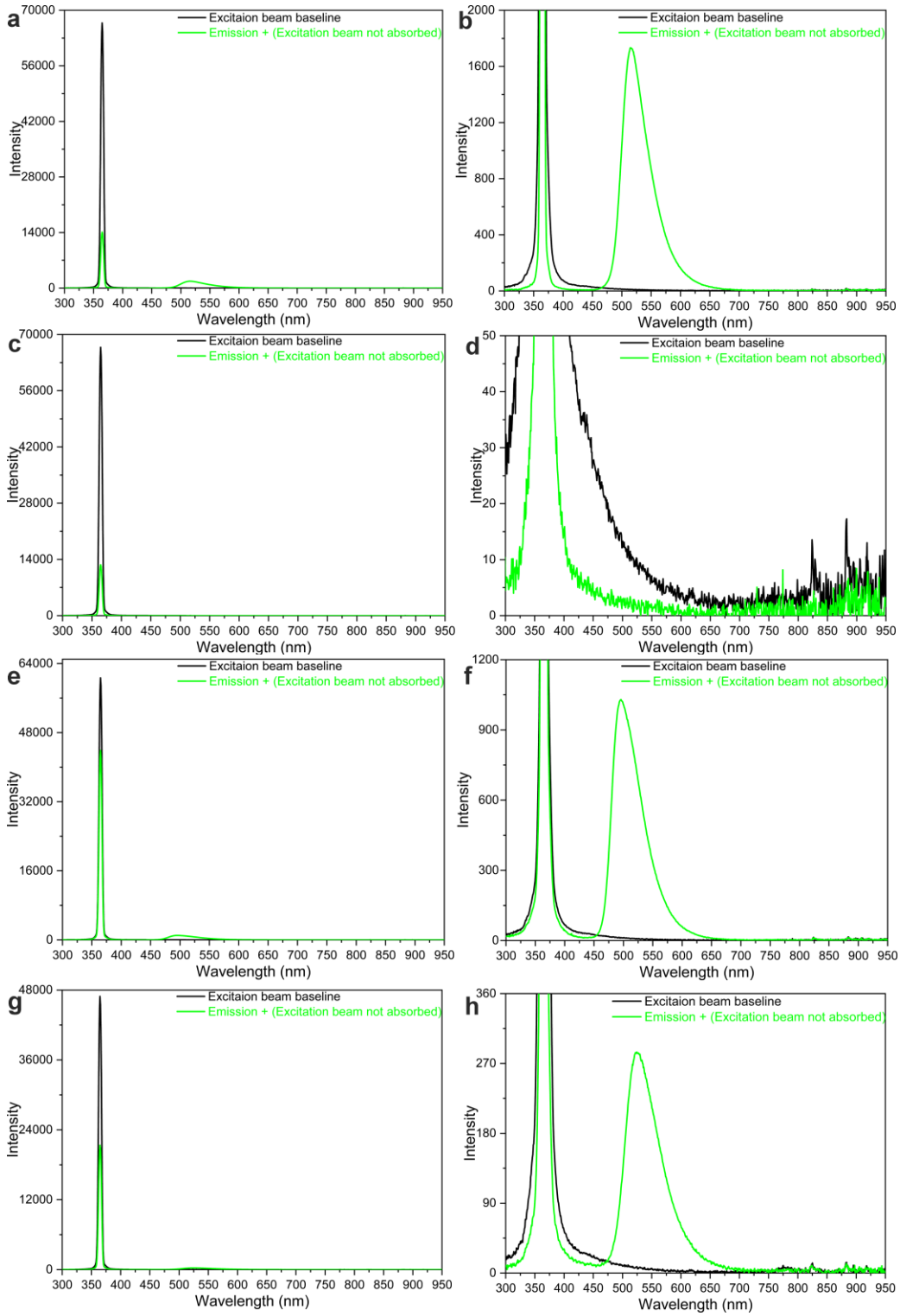

Figure S33. The emission spectra to obtain AQY: (a, b) solid-state monomer **4**; (c, d) solid-state CPF-1; (e, f) monomer **4** dispersed in THF; (g, h) CPF-1 dissolved in THF.

Aerobic oxidation of benzyl alcohol catalysis experiment:[28] 20 mg CPF-1 were dispersed in 1 mmol benzyl alcohol/ 10 mL ACN solution in a round bottom one-neck flask. 60 mL air was bubbled into ACN solution by needle/syringe to increase the oxygen concentration in solution, and then the flask was sealed with stopper/ Teflon. The suspension in flask was heated to 80 ºC with continuous stirring at 500 rpm. After specific-hours reaction, samples were collected by syringe and filtered. ^{1}H NMR was adopted to test the components in solution. However, no benzaldehyde was detected after 120 h.

Photocatalytic hydrogen evolution experiments for hydrogen was detected using Labsolar-III AG system from Beijing Perfect Light Company, consisting of four parts: a circulation line, a reactor, a vacuum section, and a control panel. Temperature controller kept the temperature at 25±1ºC. The reactor was filled with 20 mg of catalyst, 90 mL deionized water and 10 mL triethanolamine (10%) and H_2PtCl_6 (3wt%Pt) (note: we also handled experiment without adding H_2PtCl_6), degassed and then irradiated with a PLS-SXE300c 300W Xe lamp with cut off filters (wavelength 380 -780 nm), or without cut off filters (wavelength 300-2500 nm). Pressure vs. time profile was recorded and was converted to volume vs. time. The obtained gas was injected into GC7900 gas chromatograph (GC) to determine the volume%, and the amount of evolved H_2 in μmol was calculated from the volume.

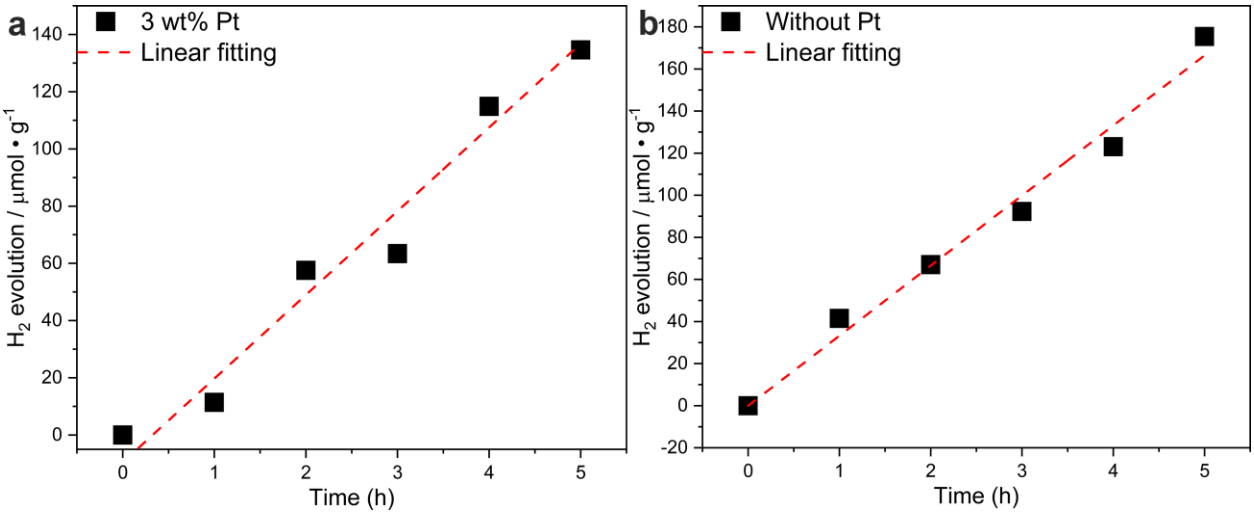

Figure S34. Hydrogen evolution of CPF-1 under light with wavelength ranging 300-2500 nm (a) from water / triethanolamine / 3 wt% Pt (b) water / triethanolamine / without Pt co-catalyst. The red lines are corresponding linear curves for the calculation of hydrogen evolution rate.

REFERENCES

1. Akdag, A.; Wahab, A.; Beran, P.; Rulisek, L.; Dron, P. I.; Ludvik, J.; Michl, J. Covalent dimers of 1, 3-Diphenylisobenzofuran for singlet fission: synthesis and electrochemistry. *J. Org. Chem.* **2014,** 80 (1), 80-89.

2. Hemavathi, B.; Ahipa, T.; Pillai, S.; Pai, R. K. Cyanopyridine based conjugated polymer-synthesis and characterization. *Polymer* **2015,** 78, 22-30.

3. Martiny, M.; Steckhan, E.; Esch, T. Cycloaddition reactions initiated by photochemically excited pyrylium salts. *Eur. J. Inorg. Chem.* **1993,** 126 (7), 1671-1682.

4. Elshafie, S. M. Note on an improved Synthesis of Pyrylium Salts from Chalcones and Ketones in the presence of boron trifluoride. *Adv. Synth. Catal.* **1982,** 324 (1), 149-154.

5. Spiliopoulos, I. K.; Mikroyannidis, J. A. Synthesis of methacrylic monomers bearing stilbenoid chromophore and their free-radical polymerization to give luminescent polymers. *Macromolecules* **2002,** 35 (19), 7254-7261.

6. Schwarz, D.; Kochergin, Y. S.; Acharja, A.; Ichangi, A.; Opanasenko, M. V.; Čejka, J.; Lappan, U.; Arki, P.; He, J.; Schmidt, J. Tailored band gaps in sulphur and nitrogen containing porous donor-acceptor polymers (SNPs). *Chem. Eur. J.* **2017,** 23 (53), 13023-13027.

7. Nelson, T. D.; Crouch, R. D. Cu, Ni, and Pd mediated homocoupling reactions in biaryl syntheses: The Ullmann reaction. *Organic Reactions* **2004,** 63, 265-555.

8. Alvaro, M.; Aprile, C.; Ferrer, B.; Garcia, H. Functional molecules from single wall carbon nanotubes. Photoinduced solubility of short single wall carbon nanotube residues by covalent anchoring of 2, 4, 6-Triarylpyrylium units. *J. Am. Chem. Soc.* **2007,** 129 (17), 5647-5655.

9. Kim, M.-S.; Phang, C. S.; Jeong, Y. K.; Park, J. K. A facile synthetic route for the morphology-controlled formation of triazine-based covalent organic nanosheets (CONs). *Polym. Chem.* **2017,** 8 (37), 5655-5659.

10. Schwarz, D.; Noda, Y.; Klouda, J.; Schwarzová-Pecková, K.; Tarábek, J.; Rybáček, J.; Janoušek, J.; Simon, F.; Opanasenko, M. V.; Čejka, J. Twinned Growth of Metal-Free, Triazine-Based Photocatalyst Films as Mixed-Dimensional (2D/3D) van der Waals Heterostructures. *Adv. Mater.* **2017,** 29 (40), 1703399.

11. Ren, S.; Bojdys, M. J.; Dawson, R.; Laybourn, A.; Khimyak, Y. Z.; Adams, D. J.; Cooper, A. I. Porous, Fluorescent, Covalent Triazine-Based Frameworks Via Room-Temperature and Microwave-Assisted Synthesis. *Adv. Mater.* **2012,** 24 (17), 2357-2361.

12. Suzuki, A. Cross-Coupling Reactions Of Organoboranes: An Easy Way To Construct C□ C Bonds (Nobel Lecture). *Angew. Chem. Int. Ed.* **2011,** 50 (30), 6722-6737.

13. Sprick, R. S.; Bonillo, B.; Sachs, M.; Clowes, R.; Durrant, J. R.; Adams, D. J.; Cooper, A. I. Extended conjugated microporous polymers for photocatalytic hydrogen evolution from water. *Chem. Commun.* **2016,** 52 (65), 10008-10011.

14. Kanter, H.; Mach, W.; Dimroth, K. 1, 1-Dihalogen-λ_5-phosphorine. *Eur. J. Inorg. Chem.* **1977,** 110 (2), 395-422.

15. Müller, C.; Wasserberg, D.; Weemers, J. J.; Pidko, E. A.; Hoffmann, S.; Lutz, M.; Spek, A. L.; Meskers, S. C.; Janssen, R. A.; van Santen, R. A. Donor-Functionalized Polydentate Pyrylium Salts and Phosphinines: Synthesis, Structural Characterization, and Photophysical Properties. *Chem. Eur. J.* **2007,** 13 (16), 4548-4559.

16. Breßler, I.; Pauw, B. R.; Thünemann, A. McSAS: software for the retrieval of model parameter distributions from scattering patterns. *J. Appl. Crystallogr.* **2015,** 48 (3), 962-969.

17. Pauw, B. R.; Pedersen, J. S.; Tardif, S.; Takata, M.; Iversen, B. B. Improvements and considerations for size distribution retrieval from small-angle scattering data by Monte Carlo methods. *J. Appl. Crystallogr.* **2013,** 46 (2), 365-371.

18. Frisch, M. J.; Trucks, G.; Schlegel, H. B.; Scuseria, G.; Robb, M.; Cheeseman, J.; Scalmani, G.; Barone, V.; Mennucci, B.; Petersson, G. Gaussian 09, revision A. 1. *Gaussian Inc. Wallingford CT* **2009,** 27, 34.

19. Weigend, F.; Ahlrichs, R. Balanced basis sets of split valence, triple zeta valence and quadruple zeta valence quality for H to Rn: Design and assessment of accuracy. *Phys. Chem. Chem. Phys.* **2005,** 7 (18), 3297-3305.

20. Kutzelnigg, W.; Fleischer, U.; Schindler, M., The IGLO-Method: ab-initio calculation and interpretation of NMR chemical shifts and magnetic susceptibilities. In *Deuterium and shift calculation*, Springer: 1990; pp 165-262.

21. Pun, C. D., *Recent advances in density functional methods*. World Scientific: 1995; Vol. 1.

22. Adamo, C.; Barone, V. Toward reliable density functional methods without adjustable parameters: The PBE0 model. *J. Chem. Phys.* **1999,** 110 (13), 6158-6170.

23. Weigend, F. Accurate Coulomb-fitting basis sets for H to Rn. *Phys. Chem. Chem. Phys.* **2006,** 8 (9), 1057-1065.

24. Cossi, M.; Rega, N.; Scalmani, G.; Barone, V. Energies, structures, and electronic properties of molecules in solution with the C-PCM solvation model. *J. Comput. Chem.* **2003,** 24 (6), 669-681.

25. Stoll, S.; Schweiger, A. EasySpin, a comprehensive software package for spectral simulation and analysis in EPR. *J. Magn. Reson.* **2006,** 178 (1), 42-55.

26. Dimroth, K., Delocalized posphorus-carbon double bonds. In *Phosphorus-Carbon Double Bonds*, Springer: 1973; pp 1-147.

27. Dimroth, K.; Heide, W. Radikale durch Oxidation von λ_5-Phosphorin-Derivaten. *Chem. Ber.* **1981,** 114 (9), 3004-3018.

28. Long, Z.; Sun, L.; Zhu, W.; Chen, G.; Wang, X.; Sun, W. P-Doped carbons derived from cellulose as highly efficient metal-free catalysts for aerobic oxidation of benzyl alcohol in water under an air atmosphere. *Chem. Commun.* **2018,** 54 (65), 8991-8994.